Published in final edited form as:
Int J Radiat Biol. 2008 December ; 84(12): 1001–1010. doi:10.1080/09553000802552143.

Synthesis and application of molecular probe for detection of hydroxyl radicals produced by $Na^{125}I$ and *γ*-rays in aqueous solution

AMARJIT SINGH, **YONGLIANG YANG**, **S. JAMES ADELSTEIN**, and **AMIN I. KASSIS**
Department of Radiology, Harvard Medical School, Boston, Massachusetts, USA

Abstract

Purpose—To synthesize *N*-(3-(3-aminopropylamino)propyl)-2-oxo-2*H*-chromene-3-carboxamide (**7**), a novel DNA-binding, coumarin-based, fluorescent hydroxylradical (˙OH) indicator and to assess its quantum efficiency compared with that of coumarin-3-carboxylic acid (**1**) and *N*1,*N*12-bis[2-oxo-2*H*-chromene-3-carbonyl]- 1,12-diamine-4,9-diazadodecane (**9**).

Materials and methods—Using computer-generated molecular modeling, **7** and **9** and their respective 7-hydroxylated derivatives **8** and **10** were docked onto DNA dodecamer d (CGCGAATTCGCG)2, the ligand–DNA complexes were energy minimized, and binding free energies and inhibition constants were calculated. Compound **7** was judged an appropriate target molecule and was synthesized. Compounds **1, 7**, and **9** were incubated with $Na^{125}I$ or irradiated with ^{137}Cs *γ*-rays, and the influence of pH, dose, type of radiation, and the concentration of indicator on fluorescence yield were determined.

Results—Non-fluorescent **7** and **9** are converted to fluorescent, 7-hydroxylated derivatives **8** and **10** after interaction with ˙OH in aqueous solution. For **1, 7**, and **9**, hydroxylation yield increases linearly with both $Na^{125}I$ dose (0–700 × 10^6 decays) and ^{137}Cs dose (0–11.0 Gy). Fluorescence induction is significantly reduced at acidic pH and the fluorescent quantum yield of **8** is ~3 times that of **2** or **10** at pH 7.0. With $Na^{125}I$ incubation and *γ*-ray irradiation, the fluorescence signal of **7** increases linearly with concentration and saturates at ~50 *μ*M.

Conclusion—Compound **7** quantifies lower concentrations of ˙OH than do **1** and **9**. This detector is therefore likely to be a good reporter of ˙OH produced within a few nanometers of DNA.

Keywords

Coumarin–polyamine probe; hydroxyl radical (˙OH)

Introduction

At the cellular level, the transformation of normal cells into cancerous cells is a complex phenomenon, involving evasion of apoptosis, self-sufficiency in cellular growth signals, insensitivity to cellular anti-growth signals, limitless replicative potential, and tissue invasion and metastasis with sustained angiogenesis (Coussens et al. 2000). Because of the multifaceted

Correspondence: Amin I. Kassis, Harvard Medical School, Armenise Building, Room D2-137, 200 Longwood Avenue, Boston, Massachusetts 02115, USA. Tel: +1 (617) 432 7777. Fax: +1 (617) 432 2419. amin_kassis@hms.harvard.edu.

Declaration of interest: The authors report no conflicts of interest. The authors alone are responsible for the content and writing of the paper.

events implicated in the process, it is difficult to accept that a single mutation can cause cancer. Although the complete mechanism of radiation-induced cancer has not been described, it is thought that radiation-induced biologic changes, such as bystander effects, adaptive responses, induction of genomic instability, and DNA strand breaks, are caused by the interaction of hydroxyl radicals (˙OH) with mammalian cell-associated molecules (Kadhim et al. 1995, Xue et al. 2002, Huang et al. 2003, Morgan 2003, Smith et al. 2003, Sowa et al. 2006, Huang et al. 2007, Morgan and Sowa 2007). Since ˙OH are short-lived and can diffuse only ~6 nm (Roots and Okada 1975), the development of DNA-binding probes that can quantify these radicals would certainly lead to a better understanding of the molecular basis of ˙OH-mediated DNA breaks and advance our comprehension of the radiobiologic effects thereof.

In past studies, we have attempted to develop molecular probes for the detection of ˙OH produced by DNA-targeted, Auger-electron-emitting atoms (Makrigiorgos et al. 1993, 1994, Chakrabarti et al. 1998). We have now selected to synthesize coumarin–polyamine-derived probes/conjugates, basing our decision on the following observations: (i) Polyamines, including spermine, exist in millimolar (mM) concentrations in mammalian cells and bind to DNA molecules without disturbing their three-dimensional structure and properties (Tabor and Tabor 1984, Drolet et al. 1986, Ha et al. 1998); (ii) molecular docking studies indicate favorable binding free energies and inhibition constants for the conjugates (see below); (iii) coumarin–polyamine analogs are likely to be soluble in aqueous solution; (iv) the fluorescence signal of coumarin is not quenched by DNA (Coleman et al. 2007); and (v) at low concentrations, polyamine does not aggregate DNA molecules.

Free radicals are produced in aqueous solution by radiolysis hydroxylate aromatic compounds including coumarin (Raghavan and Steenken 1980, Makrigiorgos et al. 1993, Kaur and Halliwell 1994). This event is influenced by the: (i) Radiation dose (10 Gy dose produces ~2.7 μM ˙OH) (von Sonntag 1987, Makrigiorgos et al. 1993); (ii) the pH of the medium (acidic pH drastically lowers the fluorescence signal); (iii) the concentration of the probe in solution; and (iv) the buffer used during irradiation. We had hypothesized that the addition of multiple coumarin groups to a given molecule would correspondingly enhance the fluorescence signal. This has not been demonstrated; in fact, the fluorescence yield for the trimer we designed is ~4-fold less than that for the dimer, the latter having a fluorescence signal approaching that of coumarin-3-carboxylic acid (Singh et al. 2007).

Herein we examine coumarin-3-carboxylic acid (**1**), *N*-(3-(3-aminopropylamino) propyl)- 2-oxo-2*H*-chromene-3-carboxamide (**7**), and N^1,N^{12}-bis[2-oxo-2*H*-chromene-3-carbonyl]-1,12-diamine-4,9-diazadodecane (**9**), incubated with $Na^{125}I$ or irradiated with γ-rays in aqueous solution. The data indicate *in situ* hydroxylation of coumarin–polyamine conjugates generates a fluorescent compound, and the intensity of the fluorescence signal is proportional to the yield of radicals. The hydroxylation yield depends on pH, dose, and compound concentration. Interestingly, **7** has greater fluorescent yield than **1** and **9**.

Materials and methods

Coumarin-3-carboxylic acid, *N*-hydroxysuccinamide, 2,4-benzaldehyde, Meldrum's acid, 1,3-dicyclohexylcarbodiimide, tetrahydrofuran, dimethyl sulfoxide (DMSO), and disposable polyacrylamide cuvettes were purchased from Sigma-Aldrich (St Louis, MO, USA). Iodine-125 (2,200 Ci/mmol) in NaOH solution was purchased from GE Healthcare Corporation (Milwaukee, WI, USA), and radioactivity was determined in a gamma counter. ^{1}H NMR (nuclear magnetic resonance) spectra were recorded on a Varian XL-200 MHz spectrometer (Palo Alto, CA, USA). Electrospray mass spectrometry was performed on a Bruker Daltonics ApexII 3T Fourier transform mass spectrometer. Fluorescence intensity was measured in an LS50B PerkinElmer spectrophotometer (Boston, MA, USA). Column chromatography was

used for routine purification of the reaction products, and the column output was monitored with thin layer chromatography (TLC) on Sigma-Aldrich fluorescent silica gel-coated glass plates.

Computational docking of coumarin–polyamine analogs with DNA

The crystal structure for oligonucleotide d(CGCGAATTCGCG)2 was obtained from the Protein Data bank (PDB code: 443D) as a *B*-DNA model. Metal ions and crystal water were retained during all simulations. The polar hydrogens of water were added, and the hydrogen bonding network was further optimized by the PDB2PQR program (Morris et al. 1998). The coumarin–polyamine ligands were energy minimized by the GROMOS molecular mechanics force field implemented in the PRODRG2 program (Schüttelkopf and van Aalten 2004), and Gasteiger charges (polar hydrogens) were assigned to the ligands with AutoDock Tools.

The polyamine chains were treated as polycationic instead of neutral to mimic the cationic properties of polyamine in a water environment. The AutoDock 3.05 program was used for all docking studies of coumarin–polyamine analogs. The advanced Lamarckian genetic algorithm (set at level 2) provided the searching method and the top 100 structures were reported. The binding free energy scoring function used by AutoDock is given by:

$$\Delta G = \Delta G_{vdw} + \Delta G_{hbond} + \Delta G_{elec} + \Delta G_{tor} + \Delta G_{sol}$$

(Morris et al. 1998)where, ΔG = total binding free energy; $\Delta Gvdw$ = van der Waals interaction energy; ΔG_{hbond} = hydrogen bonding energy; ΔG_{elec} = electrostatic energy; ΔG_{tor} = tortional free energy; ΔG_{sol} = desolvation energy. In our analysis, we selected only the best docked structures with the lowest binding free energies reported by AutoDock.

Chemical synthesis (Figure 1)

7-Hydroxy-2-oxo-2*H*-chromene-3-carboxylic acid (**2**), 2-oxo-2*H*-benzopyran-3-carboxylic acid *N*-succinimidyl ester (**3**), 7-hydroxy-2-oxo-2*H*-benzopyran-3-carboxylic acid *N*-succinimidyl ester (**4**), N^1,N^{12}-bis[2-oxo-2*H*-chromene-3-carbonyl]-1,12-diamine-4,9-diazadodecane (**9**), and N^1,N^{12}-bis[7-hydroxy-2-oxo-2*H*-chromene-3-carbonyl]-1,12-diamine-4,9-diazadodecane (**10**) were synthesized as reported previously (Singh et al. 2007). Compounds were purified and then analyzed by NMR and mass spectroscopy.

Tert-butyl 3-(3-(2-oxo-2H-chromene-3-carboxamido) propylamino)propylcarbamate (5)

Compound **5** was synthesized by stirring a mixture of **3** (6.97 mM, 2.0 g) and *tert*-butyl [3-(3-aminopropylamino)propyl]carbamate (6.34 mM, 1.465 g) in tetrahydrofuran (50 ml) for 12 h at room temperature. The crude product was purified by silica gel column chromatography. The compound was isolated in 92.73% yield (2.37 g). The structure was confirmed on the basis of ^{1}H NMR and high resolution mass spectral data. ^{1}H NMR (200 MHz, DMSO-*d*6): δ 8.86 (s, 1H), 8.79 (s (br), 1H), 7.99 (d, 1H), 7.75 (m, 1H), 7.46 (m, 2H), 3.37 (m, 2H), 2.95 (m, 2H), 2.50 (s (br), 4H), 1.66 (m, 2H), 1.51 (m, 2H), 1.36 (s, 9H). HRMS (high resolution mass spectroscopy), MALDI-tof (Matrix Assisted Laser Desorption Ionization – time of flight), ESI (electrospray ionisation): calculated (M + H) 404.2185, found (M + H) 404.2180.

Tert-butyl 3-(3-(7-hydroxy-2-oxo-2H-chromene-3-carboxamido)propylamino) propylcarbamate (6)

Compound **6** was synthesized by stirring a mixture of **4** (13.19 mM, 4.0 g) and *tert*-butyl [3-(3-aminopropylamino)propyl]carbamate (10.99 mM, 2.54 g) in tetrahydrofuran (75 ml) for 15 h at room temperature. The crude product was purified by silica gel column chromatography.

The compound was isolated in 83.92% yield (3.87 g). The structure was confirmed on the basis of ^{1}H NMR and high resolution mass spectral data. ^{1}H NMR (200 MHz, DMSO-*d*6): δ 8.72 (s (br), 1H), 8.60 (s, 1H), 7.60 (d, J = 8.8 Hz, 1H), 6.84 (s (br), 1H), 6.62 (d, J = 8.8 Hz, 1H), 6.46 (s, 1H), 3.35 (m, 2H), 2.97 (m, 2H), 2.64 (m, 2H), 1.69 (m, 2H), 1.57 (m, 2H), 1.37 (s, 9H). HRMS (MALDI-tof, ESI): calculated (M + H) 420.2134, found (M + H) 420.2130.

N-(3-(3-aminopropylamino)propyl)- 2-oxo-2H-chromene-3-carboxamide (7)

The t-Boc deprotection of **5** was used to produce **7**. Compound **5** (1.34 mmol, 500 mg) was stirred with trifluoroacetic acid (2.0 ml) and dichloromethane (10 ml). Upon completion of the hydrolysis, monitored by TLC, the solvent was evaporated under reduced pressure. The product was purified (92% yield) and analyzed by NMR and mass spectrometry. ^{1}H NMR (200 MHz, DMSO-*d6*): δ 8.85 (s, 1H), 8.59 (s, NH), 8.01 (d, 1H), 7.78 (m, 1H), 7.49 (m, 2H), 3.43 (m, 2H), 2.96 (s (br), 6H), 1.87 (m, 4H). HRMS (MALDI-tof, ESI): calculated (M + H) 304.1661, found (M + H) 304.1652.

N-(3-(3-aminopropylamino)propyl)- 7-hydroxy-2-oxo-2H-chromene-3-carboxamide (8)

The t-Boc deprotection of **6** was used to produce **8**. Compound **6** (3.10 mmol, 1.3 g) was stirred with trifluoroacetic acid (5 ml) and dichloromethane (25 ml). Upon completion of the hydrolysis, monitored by TLC, the solvent was evaporated under reduced pressure. The product was purified (yield 93.02%) and analyzed by NMR and mass spectrometry. ^{1}H NMR (200 MHz, DMSO-*d*6): δ 8.78 (s, 1H), 8.51 (s, NH), 7.82 (d, 1H), 6.89 (d, 1H), 6.82 (s, 1H), 3.40 (m, 2H), 2.94 (s (br), 6H), 1.86 (m, 4H). HRMS (MALDI-tof, ESI): calculated (M + H) 320.1610, found (M + H) 320.1622.

Na^{125}I- and γ-ray-mediated irradiation and fluorescence spectrometry of 1, 7, and 9

All solutions were prepared in 0.1 × PBS (phosphate buffered saline), pH 7.0. The samples were irradiated in duplicate at room temperature either by incubation with iodine-125 or with γ-rays from a ^{137}Cs irradiator (Gamma Cell 40, 96.3 cGy/min) at the Dana–Farber Cancer Institute. The fluorescence intensity of irradiated samples was measured at excitation wavelength 395 nm and emission wavelength 445 nm in an LS50B PerkinElmer spectrophotometer at room temperature. In the Na^{125}I studies, the induction of fluorescence was followed as a function of time. Net relative fluorescence was derived by subtracting the small but measurable fluorescence of an identically treated unirradiated sample, and the values were plotted in arbitrary units (a.u.).

Fluorescence spectrometry of 2, 8, *and* 10

The fluorescence spectra of the synthesized, 7-hydroxylated compounds **2, 8**, and **10** were determined at 0.25 μM concentration in 0.1 × PBS, pH 7.0. In addition, the fluorescence of compounds **2** and **10** at 1.0 μM concentration and compound **8** at 0.33 μM concentration was assessed at various pH between 4.0 and 10.0. Fluorescence was measured as above.

Results

Computational docking of coumarin–polyamine analogs with DNA

In the complexes of **7** and **8** with DNA, the coumarin group is buried deeply in the minor groove to pack with the deoxyribose ring of adenosine, while the amide NH group forms a hydrogen bond with the deoxyribose oxygen of thymidine (Figure 2A–2D). Detailed analysis of the docking data shows that the cationic polyamine tail contributes two polar hydrogens that bind with each oxygen atom of thymidine and one polar hydrogen that binds with the deoxyribose oxygen of cytosine. In addition to sharing a binding pose, **7** and **8** have similar binding energies, suggesting the major contribution to the binding comes from the polyamine chain. For **9** and

10 (Figure 2E–2H), one coumarin group of the dicoumarin–polyamine ligand is buried in the minor groove whereas the other coumarin group points out of the groove.

This is consistent with the finding that there seems to be no regularity of binding for polyamine compounds with DNA structure because of the high flexibility of the polyamine chain (Korolev et al. 2002). By adopting this conformation, the polar hydrogens on the polyamine chain form much stronger hydrogen bonds with the more negatively charged oxygen atoms of the phosphate diester backbone.

Consequently, the binding of **9** and **10** with DNA is ~3 kcal/mol tighter than that of **7** and **8** (Table I).

Fluorescence spectrometry and role of pH

For all compounds, emission maxima are centered at 445 nm when excitation occurs at 395 nm. The fluorescence spectra of the synthesized, 7-hydroxylated compounds **2, 8**, and **10** at pH 7.0 are found in Figure 3A. At equimolar concentrations (0.25 μM), the fluorescent quantum yield of **8** is 3.3 times that of **2** while that of **10** is slightly higher than that of **2**.

As expected, the exposure of **1, 7**, and **9** (100 μM in 0.1 × PBS, pH 7.0) to $Na^{125}I$ (2.2×10^{12} decays) and irradiation of these compounds (50 μM in 0.1 × PBS, pH 7.0) with ^{137}Cs-rays (9.4 Gy) (Figure 3B and 3C, respectively) lead to the formation of fluorescent derivatives whose emission spectra are identical to those of **2, 8** and **10**, indicating indirectly that hydroxylation takes place at the 7-position in the coumarin ring.

The effects of pH on the fluorescence yield of **2, 8**, and **10** (**2** and **10** at 1.0 μM and **8** at 0.33 μM concentration) are shown in Figure 4. At pH 4.0, all compounds have a very low fluorescence signal, indicating their inadequacy as detectors. At pH 10.0, all compounds have a high fluorescence signal with that for **2** being off-scale. From pH 6.8–7.4, **2** shows incremental increases in fluorescence signal with increase in pH, whereas the polyamine chain-containing **8** and **10** have slight changes in fluorescence signal that is probably due to the presence of the NH groups. The significant variations in fluorescence of **2** with pH could be due to a free carboxylic group directly attached to the coumarin ring whereby the abstraction of a proton leads to electron delocalization in the benzopyran ring.

Effect of $Na^{125}I$ dose and probe concentration on fluorescence signal

With incubation of **1, 7**, and **9** (100 μM, pH 7.0) in three radioactivity concentrations of $Na^{125}I$ (16.8 ± 0.2 μCi/ml, 69.5 ± 1.5 μCi/ml, and 138 ± 2 μCi/ml), the fluorescence signal is enhanced to a different extent (Figure 5).

When the fluorescence of **7** is plotted as a function of the number of decays or exposure times, the slopes at each of these three radioactivity concentrations increase with escalating radioiodine concentrations and all responses are linear with R values > 0.99 (Figure 5A–5C). For **1** and **9**, the linear slopes are similar to each other and ~3.5 times lower than those for **7**, i.e. following exposure to the same $^{\cdot}OH$ flux, the fluorescence quantum yield for **1** is 3.5 times higher than that of **9** and **1** (Figure 5A–5C). At any given time, increasing the dose amplifies the fluorescence signal. For example (Figure 5D), at 120 h and incubation with 16.8 ± 0.2, 69.5 ± 1.5, and 138 ± 2 μCi/ml, fluorescence values for **1** are 38, 150, and 230 a.u., respectively; for **7**, 150, 500, and 850 a.u., respectively; and for **9**, 38, 150, and 230 a.u., respectively. Since **7** is most responsive to radiation (because of its high fluorescence yield), this derivative was studied in more detail.

When various concentrations of **7** (1–100 μM in 0.1 × PBS, pH 7.0) are incubated with $Na^{125}I$ (79 ± 3 μCi) and the fluorescence signals plotted as a function of concentration, the

fluorescent signal increases rapidly with detector concentration and saturates at about 50 μM (Figure 6A). Plotting these data as a function of time or number of decays (Figure 6B) demonstrates linear increases in fluorescence signal (R values approximately 0.99). At 50 μM, $y = 4.38 * 10^{-10}x$.

Effect of γ-ray dose and probe concentration on fluorescence signal

Compound **7** at various concentrations (1–100 μM in 0.1 × PBS, pH 7.0) has also been irradiated with escalating doses of rays ^{137}Cs-rays (0–10.5 Gy), and the fluorescence signal has been plotted as a function of concentration (Figure 6C). As previously observed following Na^{125}I exposure, the fluorescence signal increases rapidly at the lower concentrations and plateaus around 50 μM. When these data are plotted as a function of irradiation dose (Figure 6D), a linear increase in fluorescence signal is observed with R values > 0.99.

To approximate the Na^{125}I time-mediated irradiation conditions, samples of **1, 7** and **9** (50 μM in 0.1 × PBS, pH 7.0) have been repeatedly irradiated with ^{137}Cs (total dose = ~11.0 Gy). After each dose fraction, the fluorescence is recorded, and the process is repeated. Samples were irradiated in measurement polyacrylamide cuvettes (not in glass cuvettes) and in the experimental dose range within which no darkening was observed. Our findings indicate that the fluorescence signal for the three coumarin derivatives increases linearly with increasing dose (Figure 7), and that the quantum efficiency of **8** is ~3 times higher than that of **2** and **10** (which are equal). Surprisingly and unexpectedly, the fluorescence yield following fractionated irradiation (Figure 7 – at 50 μM, $y = 79.7 * x$) is ~1.6-fold higher than that after single-dose exposures (Figure 6D – at 50 μM, $y = 50.1 * x$).

Discussion

DNA molecules are highly charged. Since this property can quench the fluorescence signal of probes and scavenge hydroxyl radicals, ·OH-detector mediated quantification of the actual radical yields is difficult (Pryor 1988, Chakrabarti et al. 1998). Therefore, the development of novel compounds with quantum efficiency is a valuable goal. The aim of the current study is to synthesize DNA-binding, coumarin-based molecular probes for the detection of ·OH and to assess and compare their quantum efficiency with that of coumarin-3-carboxylic acid (**1**). Previous work had demonstrated that the (i) benzopyran ring structure is essential for developing fluorescence-based coumarin molecular probes; (ii) γ-ray irradiation of coumarin molecules generates a fluorescent compound (7-hydroxylation in the coumarin ring); (iii) intensity of the fluorescence signal is linearly proportional to the number of 7-hydroxycoumarin molecules formed that in turn is proportional to the radiation absorbed dose; (iv) addition of multiple coumarin rings in the same molecule does not enhance the fluorescence signal in the same ratio (Singh et al. 2007).

Both Na^{125}I, used for internal irradiation, and ^{137}Cs, used for external irradiation, ionize water molecules to produce ·OH. *In situ*, ·OH react with coumarin molecules to produce hydroxylated products, including fluorescent, 7-hydroxylated coumarins. Other possible outcomes of ·OH reactions are: (i) Hydroxylation at various positions, (ii) decarboxylation of the free acid group, and (iii) cleavage of the coumarin ring, all of which leading to a decrease of the 7-hydroxylated product yield (Mead et al. 1958). The reactivity of a given ring position determines the product (hydroxylated compounds produced other than 7-hydroxylated coumarin) distribution (Goodwin and Kavanagh 1950, 1952, Crosby and Berthold 1962). In analogy, studies of benzene in aqueous solution indicate that the primary event is an electrophilic attack of the ·OH on the ring to form a hydroxycyclohexadienyl radical, after which, depending on solution conditions and the presence of oxidants, various events may take place, including decay by elimination of water, dimerization, or oxidation, thus fixing the hydroxyl moiety on the ring to give a stable product (Mantaka et al. 1971, Walling and Johnson 1975). Despite the

low yield of hydroxylated–fluorescent product, the use of coumarin derivatives is attractive because of their low cost, sensitivity, and, in principle, applicability both *in vitro* and *in vivo*.

Herein, we report that the increase in fluorescence of *N*-(3-(3-aminopropylamino)propyl)- 2-oxo-2*H*-chromene-3-carboxamide (**7**) upon incubation with $Na^{125}I$ or after γ-ray irradiation is 2–3 times that reported for (Singh et al. 2007) coumarin-3-carboxylic acid (**1**) and N^1,N^{12}-bis [2-oxo-2*H*-chromene-3-carbonyl]- 1,12-diamine-4,9-diazadodecane (**9**). A probable reason for this finding is the delocalization of an electron on the benzopyran ring by the free amine group carrying a positive charge that leaves position 7 more suitable for hydroxyl attack in **7** compared with **1** and **9**. The addition of two coumarin rings as in **9** does not affect hydroxylation. Net hydroxylation yield for the dimmer (**9)** is the same as for the monomer (**1**).

The docking studies of **7**–**10** in a DNA dodecamer demonstrate that coumarin derivatives bind in the minor groove through a combination of van der Waals and hydrogen-bonding interactions similar to the docking of *m*iodoHoechst (Chen et al. 2004) (Figure 2). Molecular modeling supports the DNA-binding properties of polyamine and further informs us that the molecule with a single coumarin ring (**7**) is buried completely in the minor groove with the deoxyribose part of adenosine and where the amide NH group forms a hydrogen bond with the deoxyribose oxygen of thymidine. With coumarin at both ends of the polyamine chain (**9**), one of the coumarins behaves similarly to the monocoumarin, whereas the other binds with the phosphate linkage in the side of DNA. Consequently, **9** and **10** have a 3 kcal/mol higher binding energy than **7** and **8**.

For **1, 7**, and **9**, incubation with $Na^{125}I$ and irradiation with γ-ray (Figure 3B and 3C, respectively) leads to the formation of compounds whose fluorescence maxima (445 nm) are similar to that of the synthetically produced 7-hydroxylated analogs (Figure 3A). Comparison of the data in Figure 3A–3C indicates that only a small fraction (~1%) of the compounds is converted into fluorescent product.

Sensitivity to pH plays an important role in fluorescence-based detection. To develop a fluorometric method, it is desirable, since fluorescence is greatly influenced by the medium pH, to scan changes in fluorescence intensity over a range of pH values for every new experimental compound. For **1**, the fluorescence signal decreases with acidic pH and increases with basic pH; for **9**, the fluorescence signal at acidic pH is negligible and, at basic pH, is similar to that at neutral pH (Figure 4). A drop in fluorescence signal between pH 8.0 and 9.0 has been reported for umbelliferone (7-hydroxycoumarin) (Goodwin and Kavanagh 1950). For **7**, the change in fluorescence signal is insignificant at or near neutral pH (6.8–7.4) (Figure 4). The fluorescence signal is influenced by both the 7-OH group and the polyamine chain; thus, accurate maintenance of pH for each compound during quantitative experiments is crucial. Molecular probes are generally used at or near neutral pH; acidic conditions are unsuitable for biologic systems.

The plot of fluorescence versus radiation dose is used as a basis for quantifying $^{\cdot}OH$ production. As seen in Figure 5, the induction of fluorescence for **1, 7** and **9** after incubation with $Na^{125}I$ is linear as a function of time and number of decays, and the fluorescence signal for **7** (at the same number of ^{125}I decays) is greater than that for **1** and **9**. With an increase in dose, the fluorescence signal is enhanced. For γ-ray irradiation, fluorescence emission of **7** is also higher than that of **1** and **9** (Figure 7).

When **7** at increasing concentrations (between 1 μM and 100 μM) is exposed to ^{125}I decays (79 ± 3 μCi) (Figure 6A and B) or irradiated with γ-rays (0–11.0 Gy) (Figure 6C and 6D), (i) the fluorescence signal rises rapidly with increases in compound concentration, and (ii) the fluorescence yield approaches saturation at ~50 μM concentration. Comparison of the ^{125}I and

γ-ray slopes at this concentration shows that each ^{125}I decay/ml deposits ~9×10^{-12} Gy when the γ-irradiated samples are exposed to a single dose (Figure 6B and 6D) and ~6×10^{-12} Gy, when the dose is fractionated over a two-day period (Figures 6B and 7).

These values agree with the calculated dose of 3.8×10^{-12} Gy/^{125}I decay (using a dose equivalent of 5.01×10^{-4} Gy/μCi-h for a 1 ml sphere of water [radius = 12,394 μm], R. W. Howell, personal communication), demonstrating the ability of these detectors to accurately report the dose. Whereas it is unclear whether this difference in dose equivalence is related to a dose-rate effect (unlike γ-ray irradiation, ^{125}I decays are accumulated over a nine-day period), exposure of these detector molecules to a source of continuous low-dose-rate radiation should lead to a more accurate estimation of ^{125}I-to-γ-ray equivalence (i.e., be more in line with the calculated value of 3.8×10^{-12} Gy). If the dose-rate effect is confirmed, it is possible that these differences may be a consequence of the higher density/concentration of ˙OH following a single dose, thereby increasing the probability of these radicals reacting with one another rather than with the coumarin molecules.

Compounds **7** and **9** are coumarin–spermine conjugates. The primary amine group at one end of **7** is an additional attractive feature of this probe as it could be chemically linked to molecules of interest (e.g., target-specific binding molecules) that enable the detection of ˙OH produced proximal to the target (e.g., intranuclear DNA). Since the binding of polyamines, including spermine, with DNA molecules (present in mM concentrations in mammalian cells) does not disturb the three-dimensional structure and properties of natural macromolecules (Tabor and Tabor 1984, Ha et al. 1998), we predict – based on the findings of our molecular docking studies and the experimental data that this coumarin derivative can be used to quantify ˙OH within the immediate vicinity of the DNA double helix in solution (~7 nm-radius cylinder) and thus advance our comprehension of the molecular basis of ˙OH-mediated DNA breaks.

Acknowledgments

This work was supported by an NRSA fellowship (A. Singh) and NIH CA 15523 (A. I. Kassis).

References

Chakrabarti S, Kassis AI, Slayter HS, Bump EA, Sahu SK, Makrigiorgos GM. Continuous detection of radiation or metal generated hydroxyl radicals within core chromatin particles. International Journal of Radiation Biology 1998;73:53–63. [PubMed: 9464477]

Chen K, Adelstein SJ, Kassis AI. Molecular modeling of the interaction of iodinated Hoechst analogs with DNA: implications for new radiopharmaceutical design. Journal of Molecular Structure: (Theochem) 2004;711:49–56.

Coleman RS, Berg MA, Murphy CJ. Coumarin base-pair replacement as a fluorescent probe of ultrafast DNA dynamics. Tetrahedron 2007;63:3450–3456.

Coussens LM, Tinkle CL, Hanahan D, Werb Z. MMP-9 supplied by bone marrow-derived cells contributes to skin carcinogenesis. Cell 2000;103:481–490. [PubMed: 11081634]

Crosby DG, Berthold RV. Fluorescence spectra of some simple coumarins. Analytical Biochemistry 1962;4:349–57. [PubMed: 14023980]

Drolet G, Dumbroff EB, Legge RL, Thompson JE. Radical scavenging properties of polyamines. Phytochemistry 1986;25:367–371.

Goodwin RH, Kavanagh F. Fluorescence of coumarin derivatives as a function of pH. Archives of Biochemistry 1950;27:152–173. [PubMed: 15419784]

Goodwin RH, Kavanagh F. The fluorescence of coumarin derivatives as a function of pH. II. Archives of Biochemistry 1952;36:422–55. [PubMed: 14944271]

Ha HC, Sirisoma NS, Kuppusamy P, Zweier JL, Woster PM, Casero RA Jr. The natural polyamine spermine functions directly as a free radical scavenger. Proceedings of the National Academy of Science of the USA 1998;95:11140–11145.

Huang L, Kim PM, Nickoloff JA, Morgan WF. Targeted and nontargeted effects of low-dose ionizing radiation on delayed genomic instability in human cells. Cancer Research 2007;67:1099–1104. [PubMed: 17283143]

Huang L, Snyder AR, Morgan WF. Radiation-induced genomic instability and its implications for radiation carcinogenesis. Oncogene 2003;22:5848–5854. [PubMed: 12947391]

Kadhim MA, Lorimore SA, Townsend KMS, Goodhead DT, Buckle VJ, Wright EG. Radiation-induced genomic instability: Delayed cytogenetic aberrations and apoptosis in primary human bone marrow cells. International Journal of Radiation Biology 1995;67:287–293. [PubMed: 7897277]

Kaur H, Halliwell B. Detection of hydroxyl radicals by aromatic hydroxylation. Methods in Enzymology 1994;233:67–82. [PubMed: 8015497]

Korolev N, Lyubartsev AP, Laaksonen A, Nordenskiöld L. On the competition between water, sodium ions, and spermine in binding to DNA: a molecular dynamics computer simulation study. Biophysical Journal 2002;82:2860–2875. [PubMed: 12023210]

Makrigiorgos GM, Baranowska-Kortylewicz J, Bump E, Sahu SK, Berman RM, Kassis AI. A method for detection of hydroxyl radicals in the vicinity of biomolecules using radiation-induced fluorescence of coumarin. International Journal of Radiation Biology 1993;63:445–458. [PubMed: 8096857]

Makrigiorgos GM, Folkard M, Huang C, Bump E, Baranowska-Kortylewicz J, Sahu SK, Michael BD, Kassis AI. Quantification of radiationinduced hydroxyl radicals within nucleohistones using a molecular fluorescent probe. Radiation Research 1994;138:177–185. [PubMed: 8183987]

Mantaka A, Marketos DG, Stein G. Continuous g and pulse radiolysis of aqueous benzene solutions: some reactions of the hydroxycyclohexadienyl radical. Journal of Physical Chemistry 1971;75:3886–3889.

Mead JAR, Smith JN, Williams RT. Studies in detoxification. 72. The metabolism of coumarin and of *o*-coumaric acid. Biochemical Journal 1958;68:67–74. [PubMed: 13522576]

Morgan WF. Non-targeted and delayed effects of exposure to ionizing radiation: II. Radiation-induced genomic instability and bystander effects *in vivo*, clastogenic factors and transgenerational effects. Radiation Research 2003;159:581–596. [PubMed: 12710869]

Morgan WF, Sowa MB. Non-targeted bystander effects induced by ionizing radiation. Mutation Research 2007;616:159–164. [PubMed: 17134726]

Morris GM, Goodsell DS, Halliday RS, Huey R, Hart WE, Belew RK, Olson AJ. Automated docking using a Lamarckian genetic algorithm and an empirical binding free energy function. Journal of Computational Chemistry 1998;19:1639–1662.

Pryor WA. Why is the hydroxyl radical the only radical that commonly adds to DNA? Hypothesis: it has a rare combination of high electrophilicity, high thermochemical reactivity, and a mode of production that can occur near DNA. Free Radical Biology and Medicine 1988;4:219–223. [PubMed: 2834274]

Raghavan NV, Steenken S. Electrophilic reaction of the OH radical with phenol. Determination of the distribution of isomeric dihydroxycyclohexadienyl radicals. Journal of the American Chemical Society 1980;102:3495–3499.

Roots R, Okada S. Estimation of life times and diffusion distances of radicals involved in X-ray-induced DNA strand breaks or killing of mammalian cells. Radiation Research 1975;64:306–320. [PubMed: 1197641]

Schüttelkopf AW, van Aalten DMF. PRODRG: A tool for high-throughput crystallography of protein–ligand complexes. Acta Crystallographica 2004;D60:1355–1363.

Singh A, Chen K, Adelstein SJ, Kassis AI. Synthesis of coumarin–polyamine-based molecular probe for the detection of hydroxyl radicals generated by gamma radiation. Radiation Research 2007;168:233–242. [PubMed: 17638412]

Smith LE, Nagar S, Kim GJ, Morgan WF. Radiation-induced genomic instability: radiation quality and dose response. Health Physics 2003;85:23–29. [PubMed: 12852467]

Sowa M, Arthurs BJ, Estes BJ, Morgan WF. Effects of ionizing radiation on cellular structures, induced instability and carcinogenesis. EXS 2006;96:293–301. [PubMed: 16383023]

Tabor CW, Tabor H. Polyamines. Annual Review of Biochemistry 1984;53:749–790.

von Sonntag, C., editor. The chemical basis of radiation biology. Taylor & Francis; London: 1987.

Walling C, Johnson RA. Fenton's reagent. V. Hydroxylation and side-chain cleavage of aromatics. Journal of the American Chemical Society 1975;97:363–367.

Xue LY, Butler NJ, Makrigiorgos GM, Adelstein SJ, Kassis AI. Bystander effect produced by radiolabeled tumor cells *in vivo*. Proceedings of the National Academy of Sciences of the USA 2002;99:13765–13770. [PubMed: 12368480]

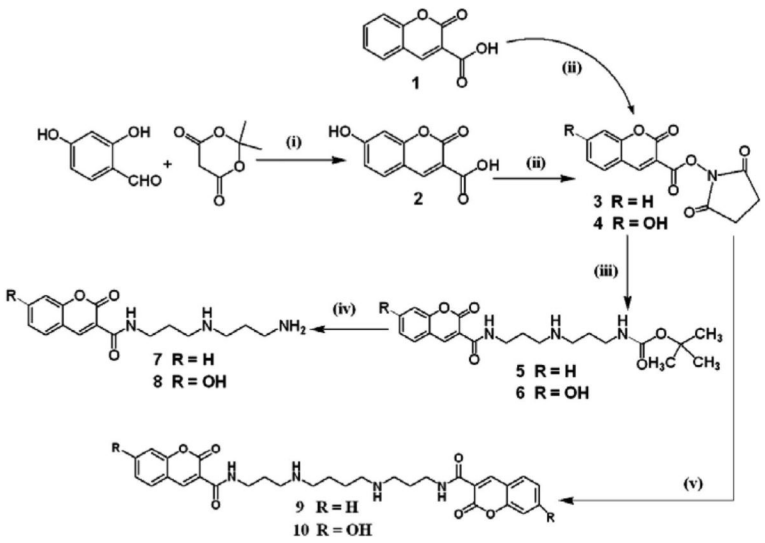

Figure 1.

Chemical pathway for synthesis of coumarin–polyamine conjugates: (i) ethanol, piperidine, acetic acid (piperidinium acetate); (ii) tetrahydrofuran, *N*-hydroxysuccinamide, 1,3-dicyclohexylcarbodiimide; (iii) tetrahydrofuran, *tert*-butyl [3-(3-aminopropylamino) propyl] carbamate; (iv) trifluoroacetic acid, dichloromethane; (v) tetrahydrofuran, spermine.

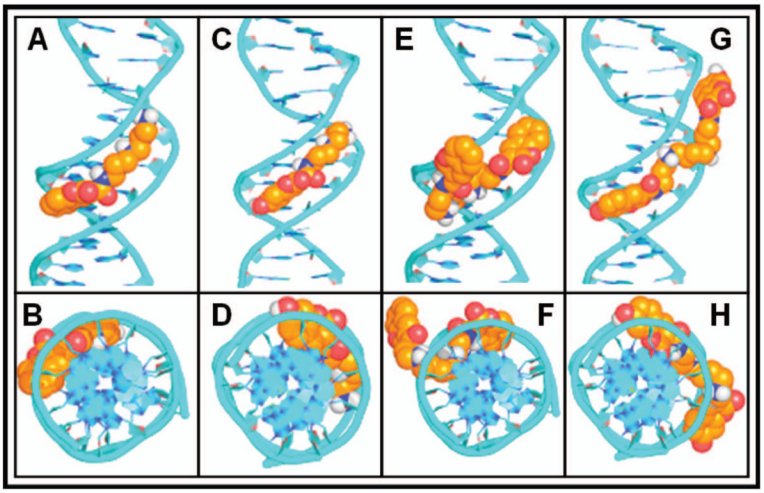

Figure 2.
Corey-Pauling-Koltun space-filling models for docking of coumarin derivatives in DNA. (A and B) **7**; (C and D) **8**; (E and F) **9**; (G and H) **10**.

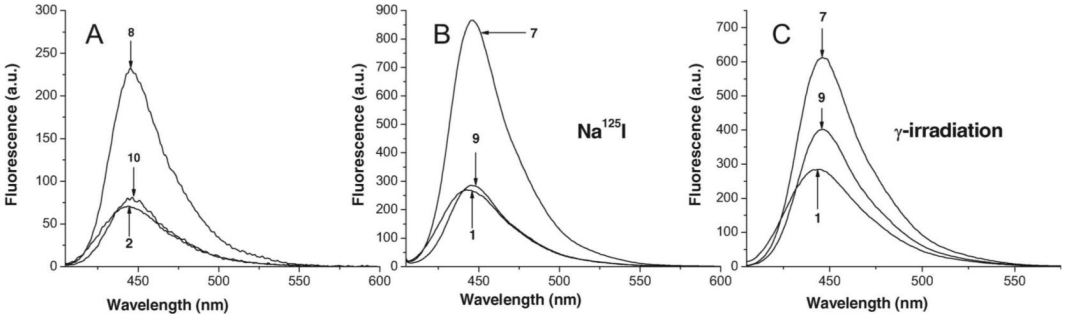

Figure 3.

(A) Emission spectra for **2, 8** and **10** (0.25 μM in 0.1 × PBS [pH 7.0]). Solutions excited at wavelength 395 nm (slit width 2.5, no. of scans 100). (B) Induction of fluorescence in **1, 7** and **9** (100 μM in 0.1 × PBS [pH 7.0]) after 120 h incubation with 138 ± 2 μCi/ml $Na^{125}I$ (6.5×10^8 decays of ^{125}I). Solutions excited at wavelength 395 nm (slit width 5.0, no. of scans 100) and fluorescence spectra quantified (400–600 nm). (C) Induction of fluorescence in **1, 7** and **9** (50 μM in 0.1 × PBS [pH 7.0]) irradiated with 9.4 Gy. Solutions excited at wavelength 395 nm (slit width 5.0, no. of scans 100) and fluorescence spectra quantified (400–600 nm).

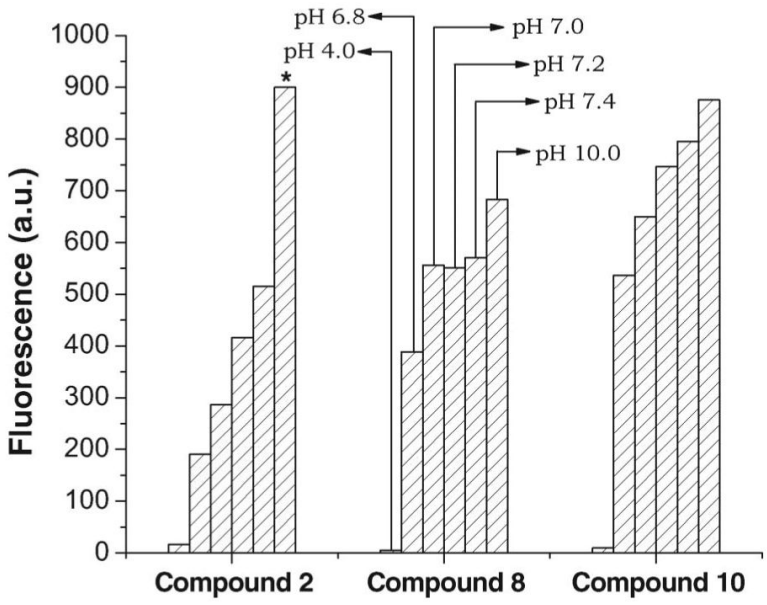

Figure 4.

Effect of pH on emission spectra of **2** and **10** at 1.0 μM concentration and **8** at 0.33 μM concentration; * indicates that value is off-scale. Net relative fluorescence in arbitrary units (a.u.) is derived by subtracting fluorescence of unirradiated samples.

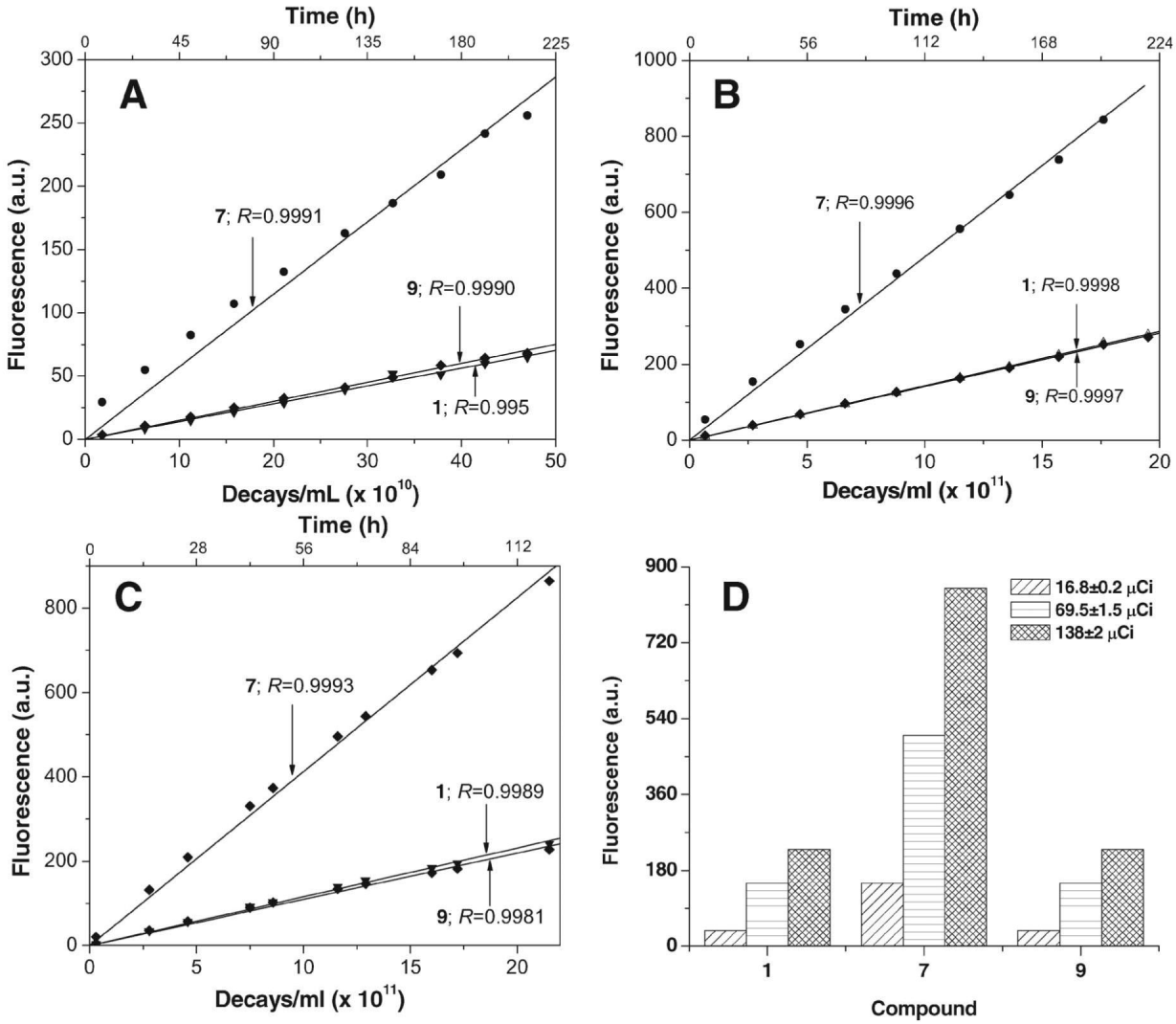

Figure 5.

(A–C) Induction of fluorescence in **1, 7**, and **9** (100 μM in 0.1 × PBS [pH 7.0]) following exposure to $Na^{125}I$: (A) 16.8 ± 0.2 μCi/ml; (B) 69.5 ± 1.5 μCi/ml; (C) 138 ± 2 μCi/ml. (D) Comparison of fluorescence for **1, 7**, and **9**, each incubated for 120 h with 16.8 ± 0.2, 69.5 ± 1.5, and 138 ± 2 μCi/ml $Na^{125}I$. Net relative fluorescence in arbitrary units (a.u.) is derived by subtracting fluorescence of unirradiated samples.

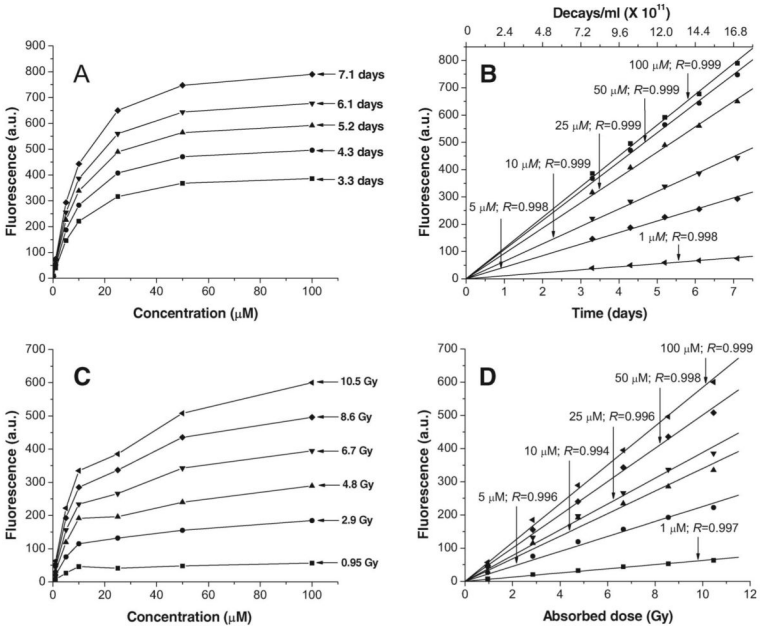

Figure 6.

Induction of fluorescence in **7** (in 0.1 × PBS [pH 7.0]) following exposure to $Na^{125}I$ (79 ± 3 μCi/ml) as function of concentration of probe (A) and time or number of decays (B). Induction of fluorescence in **7** (in 0.1 × PBS [pH 7.0]) after γ-ray irradiation as function of concentration of probe (C) and dose (D). Net relative fluorescence in arbitrary units (a.u.) is derived by subtracting fluorescence of unirradiated samples.

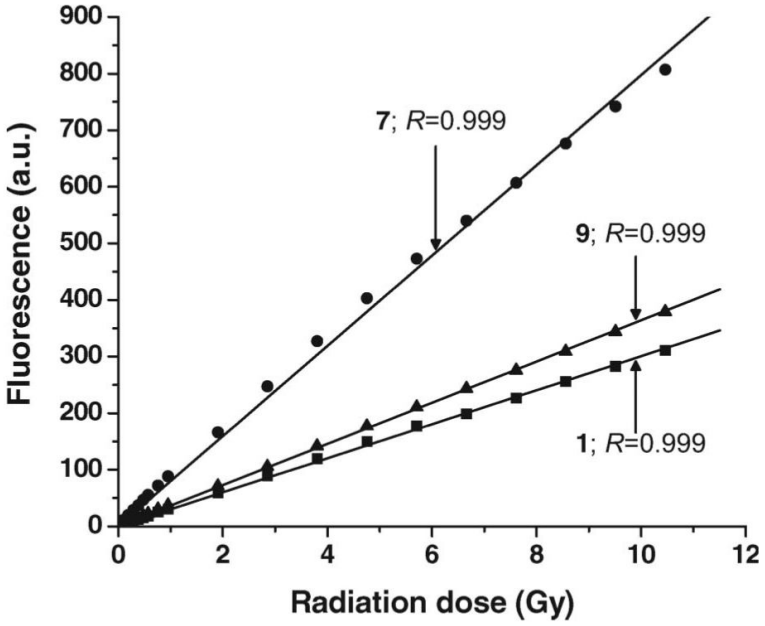

Figure 7.

Induction of fluorescence in **1, 7**, and **9** (50 μM, in 0.1 × PBS [pH 7.0]) after irradiation with escalating doses of γ-rays. Solutions were excited at wavelength 395 nm (slit width 5.0, no. of scans 100), and fluorescence was measured at 445 nm. Net relative fluorescence in arbitrary units (a.u.) is derived by subtracting fluorescence of unirradiated samples.

Table I

Predicted ΔG and K_i values for coumarin analogs

Compound	K_i[a]	ΔG[b] (kcal/mol)
7	1.04×10^{-10}	−13.62
8	1.98×10^{-10}	−13.24
9	5.39×10^{-13}	−16.74
10	2.24×10^{-12}	−15.89

[a] binding free energy

[b] inhibtion constant.